INDEX

【書籍】

【雑誌】

Wakai A, Tsuchida T, Iida H, Suzuki K.	Determination of two-photon-excitation cross section for molecular isotope separation.	*J Mol Spectrosc.*	107
de Haan S, Harms HJ, Lubberink M, Allaart CP, Danad I, Chen WJ, Diamant M, van Rossum AC, Iida H, Lammertsma AA, Knaapen P.	Parametric imaging of myocardial viability using ^{15}O-labelled water and PET/CT: comparison with late gadolinium-enhanced CMR.	*Eur J Nucl Med Mol Imaging.*	115
Iida H, Ruotsalainen U, Maki M, Haaparnata M, Bergman J, Voipio-Pulkki LM, Nuutila P, Koshino K, Knuuti J.	F-18 fluorodeoxyglucose uptake and water-perfusable tissue fraction in assessment of myocardial viability.	*Ann Nucl Med.*	121
Koshino K, Fukushima K, Fukumoto M, Sasaki K, Moriguchi T, Hori Y, Zeniya T, Nishimura Y, Kiso K, Iida H.	Breath-hold CT attenuation correction for quantitative cardiac SPECT.	*EJNMMI Res.*	133
Hirano Y, Koshino K, Watabe H, Fukushima K, Iida H.	Monte Carlo estimation of scatter effects on quantitative myocardial blood flow and perfusable tissue fraction using 3D-PET and ^{15}O-water.	*Phys Med Biol.*	141
Enmi J, Kudomi N, Hayashi T, Yamamoto A, Iguchi S, Moriguchi T, Hori Y, Koshino K, Zeniya T, Jon Shah N, Yamada N, Iida H.	Quantitative assessment of regional cerebral blood flow by dynamic susceptibility contrast-enhanced MRI, without the need for arterial blood signals.	*Phys Med Biol.*	153
Kaku Y, Iihara K, Nakajima N, Kataoka H, Fukuda K, Masuoka J, Fukushima K, Iida H, Hashimoto N.	Cerebral blood flow and metabolism of hyperperfusion after cerebral revascularization in patients with moyamoya disease.	*J Cereb Blood Flow Metab.*	173
Yoneda H, Shirao S, Koizumi H, Oka F, Ishihara H, Ichiro K, Kitahara T, Iida H, Suzuki M.	Reproducibility of cerebral blood flow assessment using a quantitative SPECT reconstruction program and split-dose ^{123}I-iodoamphetamine in institutions with different gamma-cameras and collimators.	*J Cereb Blood Flow Metab.*	183
飯田秀博, 久冨信之, 三宅義徳, 山田直明, 森田奈緒美	迅速ガスPET検査にむけて「Towards Ultra Rapid ^{15}O PET System]	*脳と循環*	191
Kikuchi-Taura A, Taguchi A, Kanda T, Inoue T, Kasahara Y, Hirose H, Sato I, Matsuyama T, Nakagomi T, Yamahara K, Stern D, Ogawa H, Soma T.	Human umbilical cord provides a significant source of unexpanded mesenchymal stromal cells.	*Cytotherapy*	199
Hirose H, Kato H, Kikuchi-Taura A, Soma T, Taguchi A.	Mouse ES cells maintained in different pluripotency-promoting conditions differ in their neural differentiation propensity.	*In Vitro Cell Dev Biol Anim.*	209
Tanaka H, Takafuji K, Taguchi A, Wiriyasermkul P, Ohgaki R, Nagamori S, Suh PG, Kanai Y.	Linkage of N-cadherin to multiple cytoskeletal elements revealed by a proteomic approach in hippocampal neurons.	*Neurochem Int.*	215
Takata M, Nakagomi T, Kashiwamura S, Nakano-Doi A, Saino O, Nakagomi N, Okamura H, Mimura O, Taguchi A, Matsuyama T.	Glucocorticoid-induced TNF receptor-triggered T cells are key modulators for survival/death of neural stem/progenitor cells induced by ischemic stroke.	*Cell Death Differ.*	226
Ohshima M, Tsuji M, Taguchi A, Kasahara Y, Ikeda T.	Cerebral blood flow during reperfusion predicts later brain damage in a mouse and a rat model of neonatal hypoxic-ischemic encephalopathy.	*Exp Neurol.*	238
Kasahara Y, Nakagomi T, Matsuyama T, Stern D, Taguchi A.	Cilostazol reduces the risk of hemorrhagic infarction after administration of tissue-type plasminogen activator in a murine stroke model.	*Stroke*	247

Tsuji M, Taguchi A, Ohshima M, Kasahara Y, Ikeda T.	Progesterone and allopregnanolone exacerbate hypoxic-ischemic brain injury in immature rats	*Exp Neurol.*	256
猪原匡史、笠原由紀子、田口明彦	「ニューロリハの最前線」細胞移植療法による神経機能回復	分子脳血管病	263
猪原匡史、田口明彦	βアミロイドの血管周囲リンパ排液路を介したクリアランス　特集「アルツハイマー病の根本的治療確立への展望」	*細胞工学*	270
Watabe T, Shimosegawa E, Watabe H, Kanai Y, Hanaoka K, Ueguchi T, Isohashi K, Kato H, Tatsumi M, Hatazawa J.	Quantitative evaluation of cerebral blood flow and oxygen metabolism in normal anesthetized rats: ^{15}O-labeled gas inhalation PET with MRI fusion.	*J Nucl Med.*	276
Kawai N, Kawanishi M, Shindou A, Kudomi N, Yamamoto Y, Nishiyama Y, Tamiya T.	Cerebral Blood Flow and Metabolism Measurement Using Positron Emission Tomography before and during Internal Carotid Artery Test Occlusions: Feasibility of Rapid Quantitative Measurement of CBF and OEF/$CMRO_2$.	*Interv Neuroradiol.*	284
Takuwa H, Masamoto K, Yamazaki K, Kawaguchi H, Ikoma Y, Tajima Y, Obata T, Tomita Y, Suzuki N, Kanno I, Ito H.	Long-term adaptation of cerebral hemodynamic response to somatosensory stimulation during chronic hypoxia in awake mice.	*J Cereb Blood Flow Metab.*	295
Unekawa M, Tomita Y, Toriumi H, Masamoto K, Kanno I, Suzuki N.	Potassium-induced cortical spreading depression bilaterally suppresses the electroencephalogram but only ipsilaterally affects red blood cell velocity in intraparenchymal capillaries.	*J Neurosci Res.*	301
Yoshihara K, Takuwa H, Kanno I, Okawa S, Yamada Y, Masamoto K.	3D analysis of intracortical microvasculature during chronic hypoxia in mouse brains.	*Adv Exp Med Biol.*	308
Masamoto K, Kawaguchi H, Ito H, Kanno I.	Dynamic two-photon imaging of cerebral microcirculation using fluorescently labeled red blood cells and plasma.	*Adv Exp Med Biol.*	316
Takuwa H, Matsuura T, Obata T, Kawaguchi H, Kanno I, Ito H.	Hemodynamic changes during somatosensory stimulation in awake and isoflurane-anesthetized mice measured by laser-Doppler flowmetry.	*Brain Res.*	322
Kawaguchi H, Masamoto K, Ito H, Kanno I.	Image-based vessel-by-vessel analysis for red blood cell and plasma dynamics with automatic segmentation.	*Microvasc Res.*	328
Masamoto K, Tomita Y, Toriumi H, Aoki I, Unekawa M, Takuwa H, Itoh Y, Suzuki N, Kanno I.	Repeated longitudinal in vivo imaging of neuro-glio-vascular unit at the peripheral boundary of ischemia in mouse cerebral cortex.	*Neuroscience.*	338

Neuromethods (2012) 71: 149–161
DOI 10.1007/7657_2012_44

Published online: 4 May 2012

Quantification of Neuroreceptors and Neurotransporters

Hiroshi Ito, Mika Naganawa, Chie Seki, Harumasa Takano, Iwao Kanno, and Tetsuya Suhara

Abstract

The binding potential relative to the concentration of nondisplaceable radiotracer in brain (BP_{ND}), corresponding to the ratio of the density of neuroreceptors or neurotransporters available to bind radiotracer in vivo (B_{avail}) to the dissociation constant of the radiotracer (K_D), can be measured by positron emission tomography (PET) with various radiotracers. PET measures the total radioactivity in brain regions, and therefore the differentiation of specific binding from the background of nondisplaceable binding is a fundamental problem in quantitative analyses of PET data. A true equilibrium condition can be obtained only by continuous intravenous infusion of radiotracer. Equilibrium condition after bolus injection of radiotracer can practically be defined as peak equilibrium at the transient moment when the specific binding is maximal. For equilibrium condition, BP_{ND} is expressed as the ratio of radiotracer concentration of specific binding to nondisplaceable binding estimated using a reference region. Kinetic analysis, which is based on the assumption that radiotracer binding can be described by the standard two-tissue compartment model, allows the differentiation of the specific binding from the background of nondisplaceable binding, therefore revealing BP_{ND}. For radiotracers with no ideal reference region, BP_{ND} can be calculated only by kinetic analysis. Distribution volumes can also be estimated by several graphic plot analyses, as well as by kinetic analysis. Graphic plot analyses can be used to distinguish graphically whether radiotracers show reversible or irreversible binding. A graphic plot analysis recently developed can also be used to distinguish graphically whether the radiotracer binding includes specific binding or not. To avoid the measurement of arterial input function, several quantitative approaches based on the use of a reference region have been developed. Both the simplified reference tissue model and multilinear reference tissue model methods were widely used to calculate BP_{ND} without the arterial input function. For each radiotracer and each purpose of PET study, an adequate quantification method should be employed.

Key words: PET, Neuroreceptor, Neurotransporter, Binding potential, Quantification

1. Introduction

There are several functions of neurotransmission in synapse (Fig. 1). The endogenous neurotransmitter is synthesized in presynaptic neuron and released into synaptic cleft. The released neurotransmitter binds to the neuroreceptors in postsynaptic membrane and then signalings are caused. The released neurotransmitter is removed

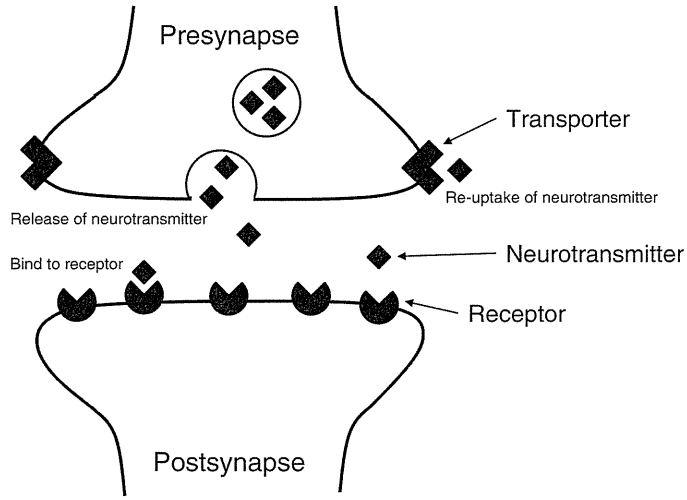

Fig. 1. Schema for functions of neurotransmission in synapse.

from synaptic cleft through the neurotransporters in presynaptic membrane. A neuroreceptor is a protein molecule in the cell membrane of neuron. For transmembrane neuroreceptors, there are two kinds of receptors, the metabotropic receptors including the G protein-coupled receptors and the ionotropic receptors. The receptors of dopaminergic and serotonergic neurotransmission system which are of main interest in pathophysiology of neuropsychiatric diseases, e.g., schizophrenia and depression, are categorized as the G protein-coupled receptors. A neurotransporter is a membrane protein in presynaptic neuron. Both pre- and postsynaptic functions can be estimated by positron emission tomography (PET) with various radiotracers. For instance, in dopaminergic neurotransmission system, the binding of dopamine receptors representing postsynaptic functions can be measured for each of D_1 and D_2 subtypes. The dopamine transporter binding and the endogenous dopamine synthesis rate representing presynaptic functions can also be measured (1). The parameters of specific binding of the radiotracer to neuroreceptors or neurotransporters consist of the density of neuroreceptors or neurotransporters available to bind radiotracer in vivo (B_{avail}) and the dissociation constant between the radiotracer and neuroreceptors or neurotransporters (K_D). The dissociation constant K_D is expressed as k_{off}/k_{on}, where k_{on} and k_{off} are equilibrium bimolecular association and dissociation rate constants between the radiotracer and neuroreceptors or neurotransporters, respectively (2).

PET measures the total radioactivity in brain regions, and therefore the differentiation of specific binding from the background of nonspecifically bound and free radiotracer is a fundamental problem in the quantitative analyses of PET data. To solve this problem, a variety of approaches have been developed for the

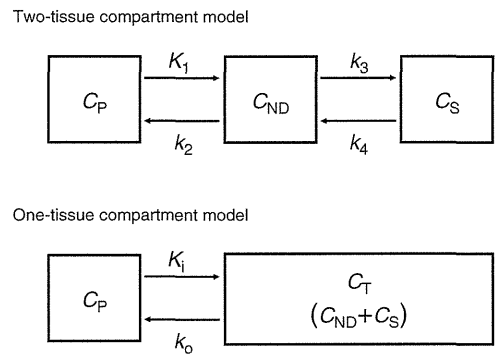

Fig. 2. The two-tissue compartment model with four rate constants and the one-tissue compartment model with two rate constants to describe the kinetics of radiotracers.

analysis of radiotracer binding. One approach is to apply a kinetic analysis that is based on the assumption that radiotracer binding can be described by the standard two-tissue compartment model (Fig. 2) (3–5). The rate constants obtained from the two-tissue compartment model can be used to calculate the curve for radiotracer concentration of specific binding (C_S) and the nonspecifically bound and free radiotracer concentration, i.e., radiotracer concentration of nondisplaceable binding (C_{ND}) in a brain region. Other approaches are based on the use of a reference region such as the cerebellum, a brain region almost devoid of neuroreceptors or neurotransporters (5, 6). The radiotracer concentration of specific binding, C_S, is defined as the difference between the total radiotracer concentration in a brain region (C_T) and the concentration in the reference region with negligible specific binding (C_R). This approach is based on the assumption that the radiotracer concentration in the reference region, C_R, is a valid estimate for that of nondisplaceable binding, C_{ND}, in a brain region with neuroreceptors or neurotransporters. In this chapter, we introduce several quantitative methods for specific binding of radiotracers to neuroreceptors or neurotransporters.

2. Equilibrium Analysis

2.1. Continuous Infusion of Radiotracer

Theoretically, a "true" equilibrium condition with constant concentration of C_T, C_S, and C_{ND} can be obtained only by continuous intravenous infusion of radiotracer (7, 8). For equilibrium condition, the ratio of B_{avail} to K_D is expressed as follows:

$$\frac{f_{ND}B_{avail}}{K_D} = \frac{C_S}{C_{ND}} = \frac{C_T - C_{ND}}{C_{ND}} \quad (1)$$

where f_{ND} is the free fraction of radiotracer in the compartment of nondisplaceable binding. $f_{ND}B_{avail}/K_D$ is defined as the binding

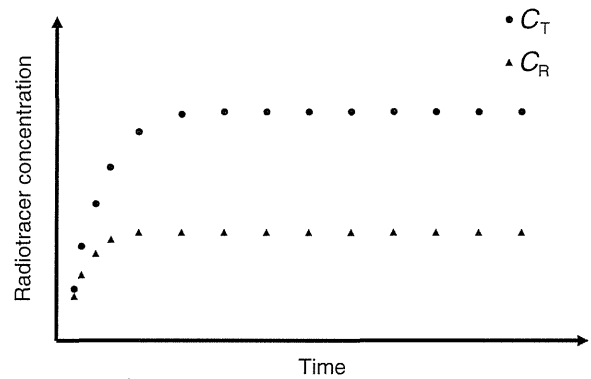

Fig. 3. The equilibrium condition obtained with an initial rapid bolus injection of radiotracer followed by continuous infusion.

potential relative to the concentration of nondisplaceable radiotracer in brain (BP_{ND}) (2, 3). When the radiotracer concentration in the reference region, C_R, is a valid estimate for C_{ND} in a brain region with neuroreceptors or neurotransporters, BP_{ND} is expressed as follows:

$$BF_{ND} = \frac{f_{ND} B_{avail}}{K_D} = \frac{C_T - C_R}{C_R} \tag{2}$$

The equilibrium condition can practically be obtained with an initial rapid bolus injection of radiotracer followed by continuous infusion using the optimal proportion between the initial rapid bolus injection and continuous infusion (Fig. 3) (8).

The concept of distribution volume has been proposed to quantitate the uptake of radiotracers in the brain during equilibrium condition. For equilibrium condition, the distribution volume is defined as the ratio of radiotracer concentration in brain to that in plasma (C_P), as follows (7):

$$V_T = \frac{C_T}{C_P} \tag{3}$$

$$V_S = \frac{C_S}{C_P} \tag{4}$$

$$V_{ND} = \frac{C_{ND}}{C_P} \tag{5}$$

where V_T is the total distribution volume, and V_S is the distribution volume with specific binding in a brain region. V_{ND} is the distribution volume with only nondisplaceable binding in a brain region and thus is devoid of specific binding sites. Using distribution volumes, BP_{ND} is expressed as follows:

$$BP_{ND} = \frac{V_T - V_{ND}}{V_{ND}} = \frac{V_T - V_R}{V_R} \tag{6}$$

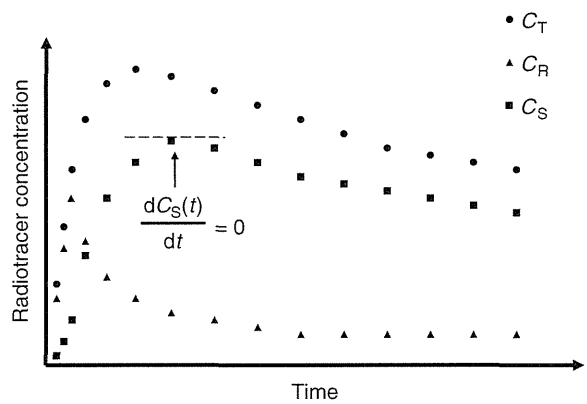

Fig. 4. The condition of peak equilibrium after bolus injection of radiotracer defined as occurring when the derivative for specific binding is zero.

where V_R is the total distribution volume in the reference region defined as C_R/C_P. When interindividual and regional differences in V_{ND} are negligibly small, V_T can be used as an indicator of BP_{ND}.

2.2. Bolus Injection of Radiotracer

Equilibrium condition after bolus injection of radiotracer can practically be defined in several ways. One approach is to assume equilibrium condition at the transient moment when the specific binding is maximal ("peak" equilibrium) (5, 6). The condition of peak equilibrium is theoretically defined as occurring when the derivative for specific binding is zero, and BP_{ND} is expressed as follows (Fig. 4):

$$BP_{ND} = \frac{C_S}{C_{ND}} \text{ when } \frac{dC_S(t)}{dt} = 0 \quad (7)$$

When the radiotracer concentration in the reference region, C_R, is a valid estimate for C_{ND} in a brain region with neuroreceptors or neurotransporters, BP_{ND} is expressed as follows:

$$BP_{ND} = \frac{C_T - C_R}{C_R} = \frac{C_S}{C_R} \text{ when } \frac{dC_S(t)}{dt} = 0 \quad (8)$$

Another approach is to assume equilibrium condition at a late time point of scan duration after rapid bolus injection of radiotracer, at which the ratio of C_S to C_{ND} is expected to approach an approximate plateau. In this condition, BP_{ND} is expressed using the radiotracer concentration in the reference region, C_R, as follows:

$$BP_{ND} = \frac{C_T - C_R}{C_R} = \frac{C_S}{C_R} \text{(at a late time point after injection)} \quad (9)$$

In PET study with rapid bolus injection of radiotracer, the total distribution volume, V_T, is defined as follows (7):

$$V_T = \frac{\int_0^\infty C_T(t)dt}{\int_0^\infty C_P(t)dt} \quad (10)$$

3. Kinetic Analysis

The time–activity curves after bolus injection of several radiotracers with high specific radioactivity have been described by the standard two-tissue compartment model with four first-order rate constants (Fig. 2) (3–5). The rate constants K_1 and k_2 describe the influx and efflux rates for radiotracer diffusion through the blood–brain barrier, respectively. The rate constants k_3 and k_4 describe the radiotracer transfer between the compartments for nondisplaceable radiotracer and specific binding. Using equilibrium bimolecular rate constants, k_3 is expressed as $f_{ND}k_{on}B_{avail}$, and k_4 is equal to k_{off}. This model can be described by the following equations:

$$\frac{dC_{ND}(t)}{dt} = K_1 C_P(t) - (k_2 + k_3)C_{ND}(t) + k_4 C_S(t) \quad (11)$$

$$\frac{dC_S(t)}{dt} = k_3 C_{ND}(t) - k_4 C_s(t) \quad (12)$$

$$C_T(t) = C_{ND}(t) + C_S(t) \quad (13)$$

The distribution volumes and BP_{ND} are expressed as follows (2, 9):

$$V_{ND} = \frac{K_1}{k_2} \quad (14)$$

$$V_T = \frac{K_1}{k_2}\left(1 + \frac{k_3}{k_4}\right) \quad (15)$$

$$BP_{ND} = \frac{k_3}{k_4} \quad (16)$$

Using the reference region, BP_{ND} can be expressed as follows:

$$BP_{ND} = \frac{V_T - V_{ND}}{V_{ND}} = \frac{V_T - V_R}{V_R} \quad (17)$$

V_R is expressed as follows:

$$V_R = \frac{K_1'}{k_2'} \quad (18)$$

where K_1' and k_2' are the influx and efflux rate constants, respectively, for the reference region with negligible k_3 and k_4. The rate constants (K_1, k_2, k_3, and k_4) can be estimated by applying a conventional nonlinear least-squares fitting procedure to the regional time–activity curves measured by PET (Fig. 5). For radiotracers with no ideal reference region, BP_{ND} can be calculated only by (16) (10). However, BP_{ND} calculated by (16) is sensitive to noise in the PET measurements as compared with that by (17) due to an interdependency of rate constants.

Binding potentials are measures of specific binding as a ratio to some other reference radiotracer concentrations. In addition to BP_{ND},

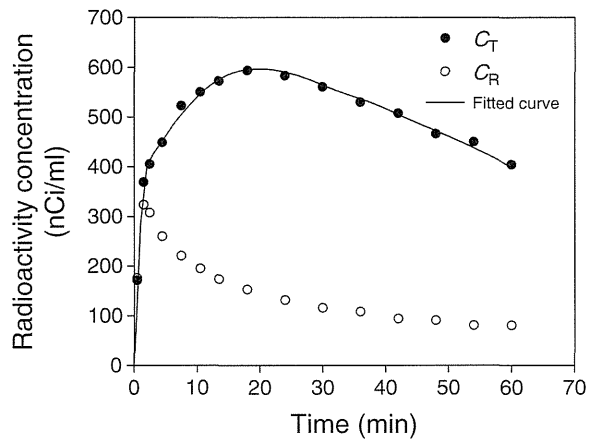

Fig. 5. Typical time–activity curve in a brain region with specific binding (C_T) and fitted curve to calculate the rate constants, K_1, k_2, k_3, and k_4. Time–activity curve in the reference region (C_R) is also shown.

the binding potential relative to the free radiotracer concentration in plasma (BP_F) and the binding potential relative to the total parent radiotracer concentration (free plus protein bound) in plasma (BP_P) are defined as follows (2):

$$BP_F = \frac{B_{avail}}{K_D} = \frac{V_T - V_{ND}}{f_P} = \frac{K_1 k_3}{f_P k_2 k_4} \tag{19}$$

$$BP_P = \frac{f_P B_{avail}}{K_D} = V_T - V_{ND} = \frac{K_1 k_3}{k_2 k_4} \tag{20}$$

where f_P is the free fraction of radiotracer in plasma.

4. Graphic Analysis

4.1. Graphic Plot Analysis by Logan et al.

The distribution volumes can also be estimated by several graphic plot analyses. An early approach was developed by Logan et al. (11, 12). The time–activity curves of radiotracers for neuroreceptors or neurotransporters have also been described by the one-tissue compartment model with two rate constants (13, 14) (Fig. 2). The rate constants K_i and k_o describe the influx and efflux rates for radiotracer diffusion through the blood–brain barrier, respectively. This model can be described by the following equation:

$$\frac{dC_T(t)}{dt} = K_i C_P(t) - k_o C_T(t) \tag{21}$$

In this model, V_T is defined as follows:

$$V_T = \frac{K_i}{k_o} \tag{22}$$

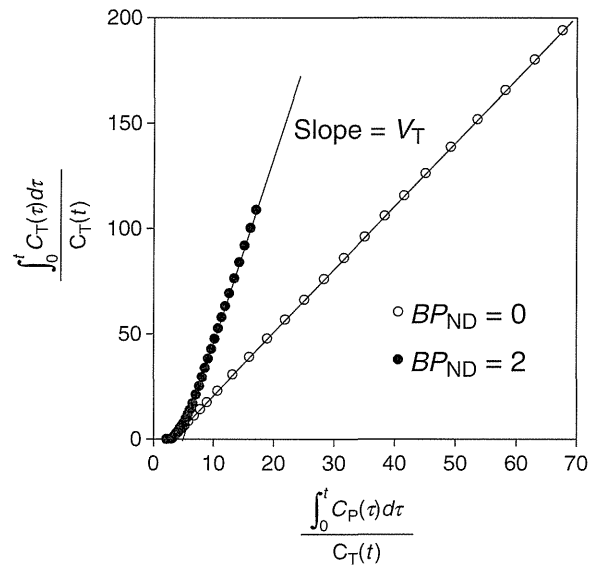

Fig. 6. Graphic plot analysis developed by Logan et al. The slope represents V_T after the equilibrium time.

The integration of (21) gives the following linear relationship:

$$Y(t) = V_T X(t) - \frac{1}{k_o} (t > t^*) \tag{23}$$

where

$$X(t) = \frac{\int_0^t C_P(\tau)d\tau}{C_T(t)}$$

$$Y(t) = \frac{\int_0^t C_T(\tau)d\tau}{C_T(t)}$$

t^* is the equilibrium time. The plot of $Y(t)$ against $X(t)$ reveals the slope representing V_T after the equilibrium time (Fig. 6). For radiotracers with irreversible binding, the slope becomes infinite in this analysis.

4.2. Graphic Plot Analysis by Ito and Yokoi et al.

A recent approach of graphic plot analysis has been developed by Ito and Yokoi et al. (15). In this approach, the following linear relationship is obtained from the integration of (21):

$$Y(t) = K_i - k_o X(t) \ (t > t^*) \tag{24}$$

where

$$X(t) = \frac{\int_0^t C_T(\tau)d\tau}{\int_0^t C_P(\tau)d\tau}$$

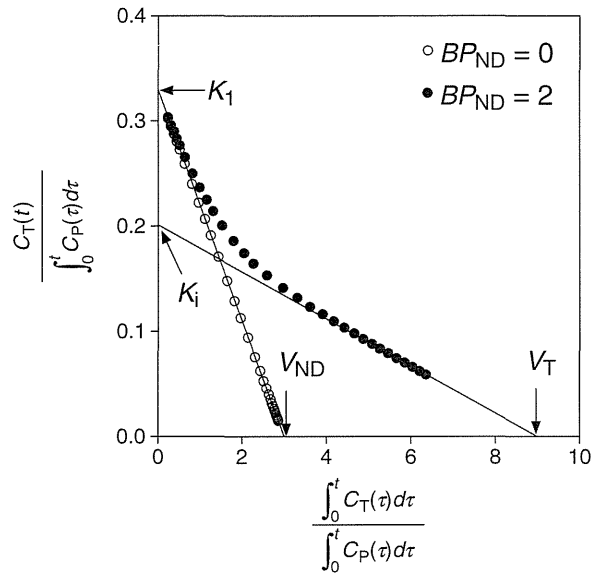

Fig. 7. Graphic plot analysis developed by Ito and Yokoi et al. When $t \rightarrow 0$, the *y*- and *x*-intercepts of the regression line represent K_1 and V_{ND}, respectively. After the equilibrium time, the *x*-intercept of the regression line represents V_T. When BP_{ND} is zero, the plot yields a straight line with a slope of $-k_2$, a *y*-intercept of K_1, and an *x*-intercept of V_{ND} through all plot data.

$$Y(t) = \frac{C_T(t)}{\int_0^t C_P(\tau)d\tau}$$

t^* is the equilibrium time. When $t \rightarrow \infty$, $X(t)$ equals V_T (7). Therefore, the plot of $Y(t)$ against $X(t)$ reaches the *x*-intercept representing V_T with a *y*-intercept for K_i after the equilibrium time (Fig. 7). In this analysis, linear regression of the plots becomes horizontal for radiotracers with irreversible binding (16).

The following equations are also obtained from the integration of (11) and (12):

$$\frac{C_T(t)}{\int_0^t C_P(\tau)d\tau} = K_1 - k_2 \frac{\int_0^t C_{ND}(\tau)d\tau}{\int_0^t C_P(\tau)d\tau} \tag{25}$$

When $t \rightarrow 0$, C_T can be considered equal to C_{ND}.

$$Y(t) = K_1 - k_2 X(t) \ (t \rightarrow 0) \tag{26}$$

where

$$X(t) = \frac{\int_0^t C_T(\tau)d\tau}{\int_0^t C_P(\tau)d\tau}$$

$$Y(t) = \frac{C_T(t)}{\int_0^t C_P(\tau)d\tau}$$

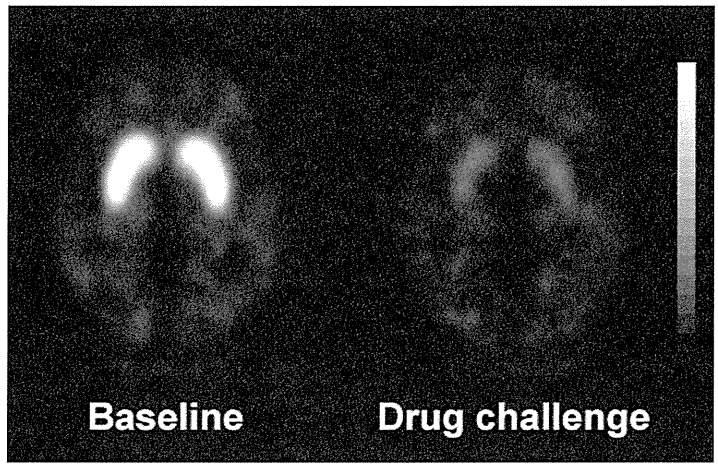

Fig. 8. Typical images of BP_{ND} in studies with [^{11}C]raclopride for baseline and drug challenge using the antipsychotic drug risperidone. After administration of antipsychotic drug, BP_{ND} decreased.

The plot of $Y(t)$ against $X(t)$ yields a straight line with a slope of $-k_2$ and a y-intercept equal to K_1 when $t \rightarrow 0$. Therefore, the x-intercept of the line represents V_{ND} (Fig. 7). In this analysis, both V_T and V_{ND}, and therefore BP_{ND}, can be estimated.

When BP_{ND} is zero, the plot of $Y(t)$ against $X(t)$ yields a straight line with a slope of $-k_2$, a y-intercept of K_1, and an x-intercept of V_{ND} through all plot data (Fig. 7) (16). Thus, this analysis can be used to distinguish graphically whether the radiotracer binding includes specific binding or not.

5. Reference Tissue Model Analysis

5.1. Simplified Reference Tissue Model

To avoid the measurement of radiotracer concentration in plasma (arterial input function), several quantitative approaches based on the use of a reference region have been developed. Using the simplified reference tissue model (SRTM), the time–activity curve in the brain region is described by that in the reference region with no specific binding, assuming that both regions have the same level of nondisplaceable radiotracer binding (17, 18):

$$C_T(t) = R_I C_R(t) + \left(k_2 - \frac{R_I k_2}{1 + BP_{ND}}\right) C_R(t) \otimes \exp\left(-\frac{k_2 t}{1 + BP_{ND}}\right) \quad (27)$$

where R_I is the ratio of K_1/K_1' (K_1, influx rate constant for the brain region; K_1', influx rate constant for the reference region). k_2 is the efflux rate constant for the brain region, and $\otimes$ denotes the

convolution integral. In this analysis, three parameters (BP_{ND}, R_I, and k_2) are estimated by a nonlinear least-squares fitting procedure. With the basis function method, these parameters can be calculated on a voxel-by-voxel basis (19, 20).

5.2. Original Multilinear Reference Tissue Model

Multilinear reference tissue model (MRTMo) is one of the graphic approaches based on the use of a reference region. After the equilibrium time *the* following linear relationship is obtained (21, 22):

$$\frac{\int_0^t C_T(\tau)d\tau}{C_T(t)} = \frac{V_T}{V_R}\frac{\int_0^t C_R(\tau)d\tau}{C_T(t)} + \frac{V_T}{V_R k_2'}\frac{C_R(t)}{C_T(t)} - \frac{1}{k_2} \quad (t>t^*) \qquad (28)$$

where V_R is the total distribution volume for the reference region, and k_2' is the efflux rate constant for the reference region. In this analysis, three parameters (V_T/V_R, k_2, and k_2'), and therefore BP_{ND}, are obtained by multiple regression analysis.

6. Occupancy of Neuroreceptors or Neurotransporters by Psychotropic Drug

The effects of antipsychotics or antidepressants have been considered to be mediated by blockade of dopamine D_2 receptors or serotonin transporters, respectively. The occupancy of dopamine D_2 receptors or serotonin transporters by antipsychotics or antidepressants can be measured by PET studies under resting condition (baseline study) and administration of psychotropic drug (drug challenge study) (23–25). The occupancy of neuroreceptors or neurotransporters is calculated as follows:

$$\text{Occupancy}(\%) = 100 \times \frac{BP_{ND(\text{Baseline})} - BP_{ND(\text{Drug})}}{BP_{ND(\text{Baseline})}} \qquad (29)$$

where $BP_{ND(\text{Baseline})}$ is BP_{ND} in the baseline study, and $BP_{ND(\text{Drug})}$ is BP_{ND} in the drug challenge study. Because almost all psychotropic drugs show reversible binding to neuroreceptors or neurotransporters same as radiotracers, $BP_{ND(\text{Drug})}$ is expressed as follows (26):

$$BP_{ND(\text{Drug})} = \frac{f_{ND} B_{avail}}{K_D\left(1 + \frac{D_{(\text{Drug})}}{K_{D(\text{Drug})}}\right)} \qquad (30)$$

where $D_{(\text{Drug})}$ is the concentration of psychotropic drug in brain tissue, and $K_{D(\text{Drug})}$ is the dissociation constant between the psychotropic drug and neuroreceptors or neurotransporters. Typical images of BP_{ND} for baseline and drug challenge studies with [^{11}C]raclopride, a radiotracer for dopamine D_2 receptors, are shown in Fig. 8.

7. Conclusion

We introduced several quantitative methods for specific binding of radiotracers to neuroreceptors or neurotransporters. A true equilibrium condition can be obtained only by intravenous continuous infusion of radiotracer. Equilibrium condition after bolus injection of radiotracer can practically be defined as peak equilibrium at the transient moment when the specific binding is maximal. During equilibrium condition, BP_{ND} can be calculated using a reference region. Kinetic analysis, which is based on the assumption that radiotracers' binding can be described by the standard two-tissue compartment model, allows us to differentiate specific binding from the background of nondisplaceable binding, therefore revealing BP_{ND}. The distribution volumes can also be estimated by several graphic plot analyses, besides the kinetic analysis. Graphic plot analyses can be used to distinguish graphically if radiotracers show reversible or irreversible binding. To avoid the measurement of arterial input function, several quantitative approaches based on the use of a reference region have been developed. Both the SRTM and MRTMo methods were widely used to calculate BP_{ND} without the arterial input function. For each radiotracer and each purpose of PET study, an adequate quantification method should be employed.

Acknowledgments

The assistance of members of the National Institute of Radiological Sciences staff in performing the PET experiments is gratefully acknowledged.

References

1. Ito H et al (2008) Normal database of dopaminergic neurotransmission system in human brain measured by positron emission tomography. Neuroimage 39:555–565
2. Innis RB et al (2007) Consensus nomenclature for in vivo imaging of reversibly binding radioligands. J Cereb Blood Flow Metab 27:1533–1539
3. Mintun MA et al (1984) A quantitative model for the in vivo assessment of drug binding sites with positron emission tomography. Ann Neurol 15:217–227
4. Huang SC et al (1986) Neuroreceptor assay with positron emission tomography: equilibrium versus dynamic approaches. J Cereb Blood Flow Metab 6:515–521
5. Farde L et al (1989) Kinetic analysis of central [^{11}C]raclopride binding to D_2-dopamine receptors studied by PET-a comparison to the equilibrium analysis. J Cereb Blood Flow Metab 9:696–708
6. Ito H et al (1998) Comparison of the transient equilibrium and continuous infusion method for quantitative PET analysis of [^{11}C]

raclopride binding. J Cereb Blood Flow Metab 18:941–950

7. Lassen NA (1992) Neuroreceptor quantitation in vivo by the steady-state principle using constant infusion or bolus injection of radioactive tracers. J Cereb Blood Flow Metab 12:709–716
8. Carson RE et al (1993) Comparison of bolus and infusion methods for receptor quantitation: application to [^{18} F]cyclofoxy and positron emission tomography. J Cereb Blood Flow Metab 13:24–42
9. Laruelle M et al (1994) SPECT quantification of [^{123}I]iomazenil binding to benzodiazepine receptors in nonhuman primates: I. Kinetic modeling of single bolus experiments. J Cereb Blood Flow Metab 14:439–452
10. Ikoma Y et al (2007) Quantitative analysis for estimating binding potential of the peripheral benzodiazepine receptor with [^{11} C]DAA1106. J Cereb Blood Flow Metab 27:173–184
11. Logan J et al (1990) Graphical analysis of reversible radioligand binding from time-activity measurements applied to [N-^{11} C-methyl]-(-)-cocaine PET studies in human subjects. J Cereb Blood Flow Metab 10:740–747
12. Logan J et al (1996) Distribution volume ratios without blood sampling from graphical analysis of PET data. J Cereb Blood Flow Metab 16:834–840
13. Koeppe RA et al (1991) Compartmental analysis of [^{11} C]flumazenil kinetics for the estimation of ligand transport rate and receptor distribution using positron emission tomography. J Cereb Blood Flow Metab 11:735–744
14. Ito H et al (1996) A simple method for the quantification of benzodiazepine receptors using iodine-123 iomazenil and single-photon emission tomography. Eur J Nucl Med 23:782–791
15. Ito H et al (2010) A new graphic plot analysis for determination of neuroreceptor binding in positron emission tomography studies. Neuroimage 49:578–586
16. Yokoi T et al (1993) A new graphic plot analysis for cerebral blood flow and partition coefficient with iodine-123-iodoamphetamine and dynamic SPECT validation studies using oxygen-15-water and PET. J Nucl Med 34:498–505
17. Lammertsma AA et al (1996) Comparison of methods for analysis of clinical [^{11} C]raclopride studies. J Cereb Blood Flow Metab 16:42–52
18. Lammertsma AA, Hume SP (1996) Simplified reference tissue model for PET receptor studies. Neuroimage 4:153–158
19. Gunn RN et al (1997) Parametric imaging of ligand-receptor binding in PET using a simplified reference region model. Neuroimage 6:279–287
20. Cselenyi Z et al (2006) A comparison of recent parametric neuroreceptor mapping approaches based on measurements with the high affinity PET radioligands [^{11} C]FLB 457 and [^{11} C] WAY 100635. Neuroimage 32:1690–1708
21. Ichise M et al (1996) Noninvasive quantification of dopamine D_2 receptors with iodine-123-IBF SPECT. J Nucl Med 37:513–520
22. Ichise M et al (2003) Linearized reference tissue parametric imaging methods: application to [^{11} C]DASB positron emission tomography studies of the serotonin transporter in human brain. J Cereb Blood Flow Metab 23:1096–1112
23. Farde L et al (1988) Central D_2-dopamine receptor occupancy in schizophrenic patients treated with antipsychotic drugs. Arch Gen Psychiatr 45:71–76
24. Suhara T et al (2003) High levels of serotonin transporter occupancy with low-dose clomipramine in comparative occupancy study with fluvoxamine using positron emission tomography. Arch Gen Psychiatr 60:386–391
25. Ito H et al (2009) No regional difference in dopamine D_2 receptor occupancy by the second-generation antipsychotic drug risperidone in humans: a positron emission tomography study. Int J Neuropsychopharmacol 12:667–675
26. Endres CJ et al (1997) Kinetic modeling of [^{11} C]raclopride: combined PET-microdialysis studies. J Cereb Blood Flow Metab 17: 932–942

Ann Nucl Med (2013) 27:25–36
DOI 10.1007/s12149-012-0655-7

ORIGINAL ARTICLE

Three-dimensional brain phantom containing bone and grey matter structures with a realistic head contour

Hidehiro Iida · Yuki Hori · Kenji Ishida · Etsuko Imabayashi · Hiroshi Matsuda · Masaaki Takahashi · Hirotaka Maruno · Akihide Yamamoto · Kazuhiro Koshino · Junichiro Enmi · Satoshi Iguchi · Tetsuaki Moriguchi · Hidekazu Kawashima · Tsutomu Zeniya

Received: 25 June 2012 / Accepted: 9 September 2012 / Published online: 26 September 2012

Abstract
Introduction A physical 3-dimensional phantom that simulates PET/SPECT images of static regional cerebral blood flow in grey matter with a realistic head contour has been developed. This study examined the feasibility of using this phantom for evaluating PET/SPECT images.
Methods The phantom was constructed using a transparent, hydrophobic photo-curable polymer with a laser-modelling technique. The phantom was designed to contain the grey matter, the skull, and the trachea spaces filled with a radioactive solution, a bone-equivalent solution of K_2HPO_4, and air, respectively. The grey matter and bone compartments were designed to establish the connectivity. A series of experiments was performed to confirm the accuracy and reproducibility of the phantom using X-ray CT, SPECT, and PET.
Results The total weight was 1997 ± 2 g excluding the inner liquid, and volumes were 563 ± 1 and 306 ± 2 mL, corresponding to the grey matter and bone compartments, respectively. The apparent attenuation coefficient averaged over the whole brain was 0.168 ± 0.006 cm^{-1} for Tc-99 m, which was consistent with the previously reported value for humans (0.168 ± 0.010 cm^{-1}). Air bubbles were well removed from both grey-matter and bone compartments, as confirmed by X-ray CT. The phantom was well adapted to experiments using PET and SPECT devices.
Conclusion The 3-dimensional brain phantom constructed in this study may be of use for evaluating the adequacy of SPECT/PET reconstruction software programs.

Keywords Brain phantom quality control · SPECT · PET · Attenuation correction

H. Iida (✉) · Y. Hori · K. Ishida · A. Yamamoto · K. Koshino · J. Enmi · S. Iguchi · T. Moriguchi · H. Kawashima · T. Zeniya
Department of Investigative Radiology, National Cerebral and Cardiovascular Center Research Institute, 5-7-1 Suita City, Osaka 565-8565, Japan
e-mail: iida@ri.ncvc.go.jp

E. Imabayashi · H. Matsuda
Saitama Medical University International Medical Center, Hidaka City, Japan

M. Takahashi
Nakamura Memorial Hospital, Sapporo City, Japan

H. Maruno
Toranomon Hospital, Tokyo, Japan

Introduction

SPECT and PET can provide volumetric images of radiolabelled ligands' distributions in living organs, reflected by biological and/or biochemical functions. Several procedures need to be adequately taken into account, in order to achieve quantitative reconstruction, including corrections for inhomogeneous detector sensitivity, dead time, attenuation and scatter in the object [1–5], motion of the object [6–8], systematic errors attributed to limited spatial resolution of the imaging devices relative to the object size (or partial volume effect, PVE) [9, 10], etc. Adequacy of the entire procedures can be evaluated using physical phantoms that simulate geometrical configurations. The Hoffman 3-dimensional brain phantom [11] has also been utilized for this purpose, as this phantom simulates the static cerebral perfusion of the grey and white matter. The digital design of the cortical grey matter in the phantom is referred as a gold standard of the reconstructed images. Inter-institutional reproducibility is also an issue, as Joshi

et al. [12] intended to minimize the inter-institutional variation of images of Hoffman 3-dimensional phantom in a multicentre clinical study using PET devices supplied from different vendors.

The Hoffman 3-dimensional brain phantom is however limited attributed to its cylindrical outer structure rather than a realistic brain contour, and also to the bone or skull structure not being taken into account. These two factors are particularly important if one intends to apply it for evaluating SPECT images, because the attenuation coefficient map is usually estimated from the head contour by assuming a uniform attenuation coefficient value throughout the head object. Effects of errors in this process on errors in the reconstructed images could not be evaluated if the Hoffman 3-dimensional phantom is utilized. It is essential for the phantom to contain a fine 3-dimensional distribution of cerebral radioactivity with the skull and a realistic head contour.

This study was aimed at developing a 3-dimensional brain phantom that simulates a static cerebral blood flow distribution in the grey matter with an inclusion of the skull structure and a realistic head contour. A recently developed photo-curable laser-modelling technique with the lipophilic resin material was employed, so that the phantom contains liquid solutions for radioactivity and the bone-equivalent contrast agent. Attention was made in the construction procedures to avoid the supporting structures, so that the whole volume of the inner spaces of the phantom can be entirely filled with liquid. We also intended to establish the connectivity of liquid space so that air bubbles are to be removed. We then evaluated the feasibility of using this phantom in typical SPECT and PET imaging.

Materials and methods

Phantom design and construction

The phantom was made of a transparent photo-curable polymer, or polyepoxide with a density of 1.07 g/mL (TSR-829, CMET Inc., Yokohama City, Japan). This material has been optimized to improve its anti-water absorbing characteristics [13]. According to precise material elements, the database for the photon cross sections (XCOM) from the National Institute of Standards and Technology (http://physics.nist.gov/PhysRefData/Xcom/html/xcom1.html) estimated that the attenuation coefficients for 511, 159, and 140 keV were 0.101, 0.157, and 0.164 cm^{-1}, respectively. The phantom was constructed using a stereo-lithographic machine with the laser-modelling technique (model RM-6000, CMET Inc, Yokohama City, Japan), which can produce the 3-dimensional construction in 50 mμ resolution. It was intended not to include any supporting structures in the inner spaces. The manufacturing speed was decreased during the laser-beam construction, so as to ensure the solidity of the phantom, thus avoiding the possible distortion of the inner structure.

The procedures to construct the 3-dimensional phantom are illustrated in Fig. 1. The basic design of the phantom was first generated using a set of T1-weighted MR images of brain obtained from a healthy 26-year-old Japanese male volunteer. The specific sequence included the gradient echo with inversion recovery, which provided gap-less, tomographic images at 1.0-mm intervals. MR images were first segmented using a K-means procedure. Then, the head contour, skull regions, ventricular regions, tracheal air space, and grey and white matter segments were manually illustrated on the computer screen, in a 2-dimensional tomographic domain (Fig. 1a). The grey matter segment included the frontal, parietal, posterior, and temporal cortex areas with the striatum, thalamus, and mid-brain regions. The image size was 440 × 440 pixels (0.5 mm/pixel), and 51 slices were acquired at 3.6-mm axial slice intervals over the whole phantom. The grey matter structure was covered in 34 total slices. During the illustration procedure, a modification was made to remove global distortions in the head and brain structures and to fit a 3-dimensional head model. The tomographic data were then exported to a 3-dimensional computer-aided design (CAD) software (Rapidform2006-sp1, INUS Technology Inc., Seoul, South Korea). The volumetric data were then interpolated in the axial direction (see Fig. 1b). The grey matter and bone compartments were designed so that they could be filled with liquid solutions, and the remaining area, except for the tracheal space, was filled with a polymer resin (see Fig. 2). The grey matter component can be filled with a radioactive solution, and the skull region is typically filled with a bone-equivalent solution of K_2HPO_4 as suggested in an earlier study [14]. The white matter region was not to be filled with liquid but was made of a photo-curable polymer, and thus the white matter region became identical to the CSF and scalp. An attention was made to avoid closed areas in the grey matter and bone segments, so that every part of the compartments could be filled with liquid. The radioactive liquid and K_2HPO_4 solution can then be diluted into each of the two compartments. In addition, no supporting resin materials were placed both in the grey matter and skull components, although the standard procedure is to place fine pillars to support the fine structure particularly for horizontal wall. The speed of the stereo-lithographic manufacturing process was slowed down, with increased pitch (Fig. 1c). The manufacturing process required whole 3 days to complete. In total, five sets of phantoms were constructed. Of these, two sets were constructed at the same time from the first

lot, while the other three were generated from the second lot.

Evaluation of the phantom

The weight and height of the phantom, as well as volumes of the grey matter and skull compartments were measured for all 5 phantoms. The phantoms were then scanned by X-ray CT using a Symbia T6 CT/SPECT hybrid scanner (Siemens, Chicago, IL, USA) without filling the phantom with liquid. The pixel size of the X-ray CT was 0.5×0.5 mm^2, and the slice pitch was 1.5 mm. The agreement between the X-ray CT and digital design, and the consistency across the five phantoms were evaluated. Additional intention was whether the wall inside the phantom is smoothly constructed or not. Distilled water was mixed with a small amount of detergent and the grey matter compartment of a phantom was filled with it. The skull compartment was filled with the K_2HPO_4 solution at the suggested concentration [14]. Both compartments were scanned again using X-ray CT. The X-ray CT images were investigated whether air bubbles remained in the phantom or not.

A transmission scan was carried out on these phantoms using a 3-headed gamma camera (Toshiba GCA-9300, Tokyo, Japan) fitted with 400-mm focal length, low energy, high resolution, symmetric fan beam collimators (N2) from the same vendor. The procedures have been described in our earlier protocol [2, 15, 16] and were shown to provide an accurate attenuation μ map of the object [2, 15, 16]. The 132-mm rotation radius used in these studies resulted in a reconstructed field of view (FOV) with a 22-cm diameter

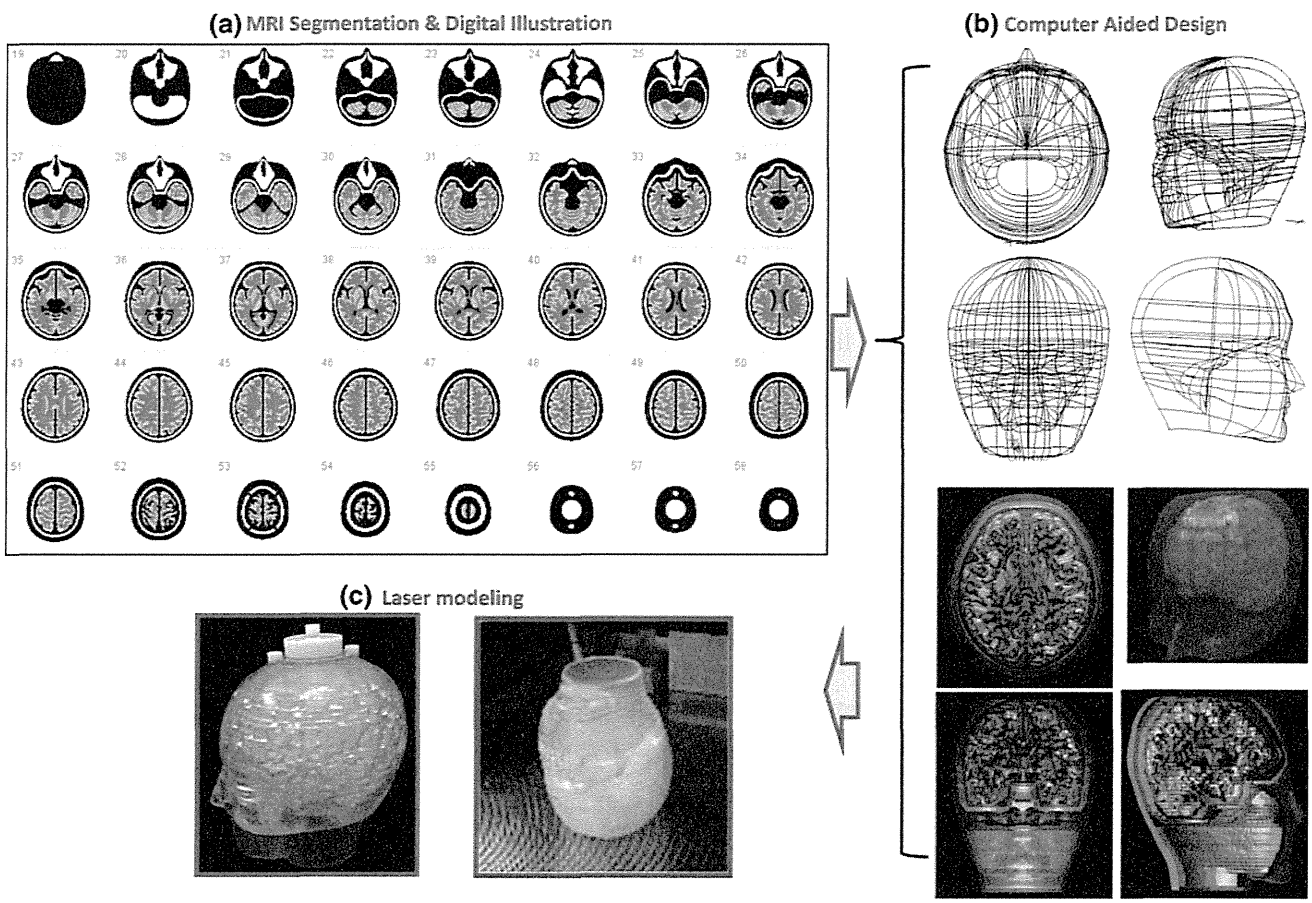

Fig. 1 Illustrative procedures to develop the 3-dimensional brain phantom. **a** Tomographic images including the cortical grey matter, deep grey matter, white matter, cerebral spinal fluid space, skull, scalp and trachea regions that were generated at 3.6-mm intervals from anatomical MR images of a young healthy volunteer. Data were manually modified to fit to a head model. **b** Three-dimensional data were then generated using the computer-aided-design software, and modifications were made to guarantee the connectivity of both the grey matter and bone compartments. Careful attention was made to establish a liquid flow stream within the structure so that air bubbles could be easily removed from the liquid space. **c** A laser-modelling technique with a stereo-lithographic machine and a photo-curable material was employed to construct the 3-dimensional phantom. There was special attention to avoid contamination from the resin-based supporting material inside the grey matter and skull compartments, and also to make the inner wall surface of the phantom as smooth as possible. The speed and pitch of the machine as well as the temperature and humidity were optimized

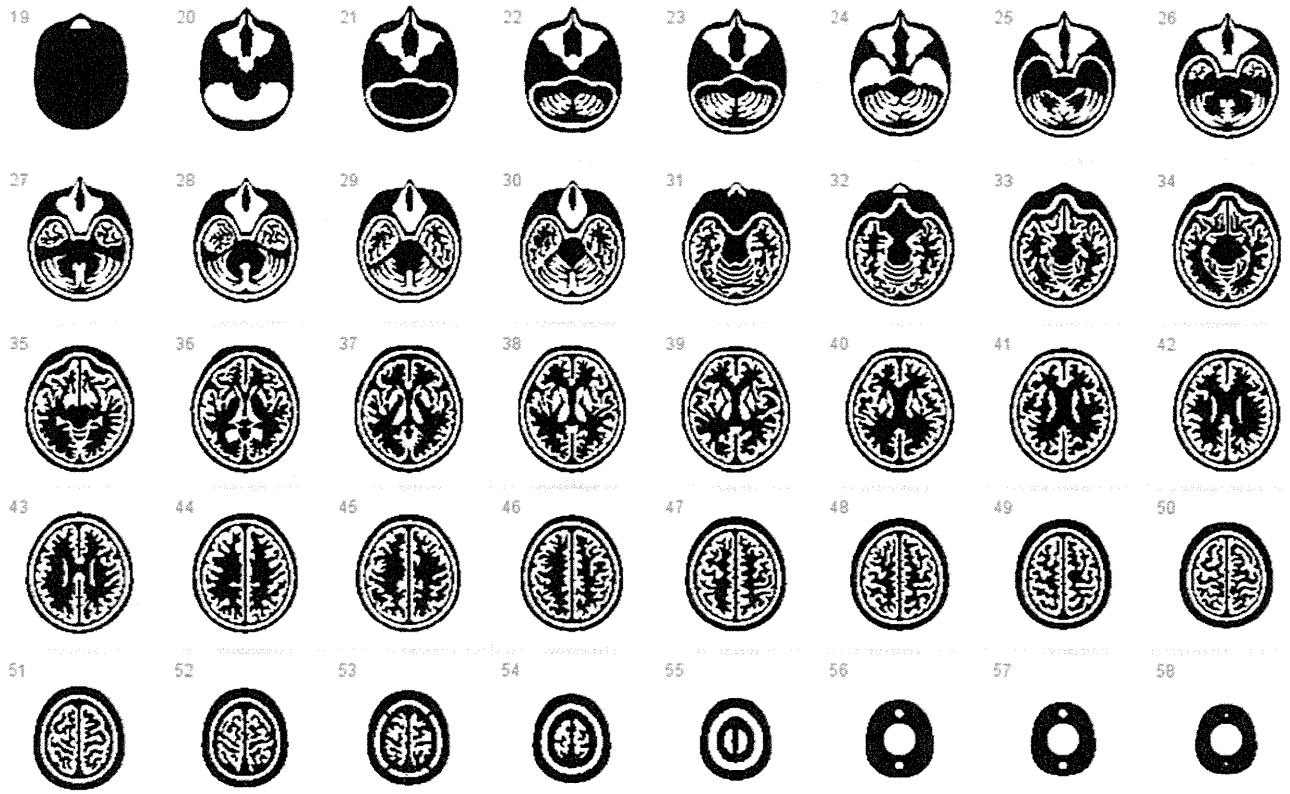

Fig. 2 Digital design of the phantom on a 2-dimensional domain. The *areas in white* correspond to the air space, which may be filled with the radioactive solution and K_2HPO_4 solution for the grey matter and skull compartments, respectively. The additional air space corresponds to the trachea

[15]. One head was used for the transmission scan, and a 25-cm long ^{99m}Tc rod source (74 MBq) was placed at the focal line of its collimator. After a 15-min blank scan, transmission projection data were collected for 15 min. The SPECT cameras were continuously rotated to collect 90 projections over 360° (10 s/projection). The energy window selected was 20 % on 140 keV. After compensating for the radioactive decay of the ^{99m}Tc, the inverse of the projection data was multiplied by the blank projection data, to which the filtered-back projection program was applied to reconstruct images of the attenuation coefficients.

SPECT/PET acquisition

Two sets of SPECT scans were performed on a phantom using a Symbia T6 scanner from Siemens (Chicago, IL, USA) fitted with a low-energy high-resolution (LEHR) collimator set. In the first experiment, the grey matter compartment was filled with a ^{99m}Tc solution of approximately 20 MBq, while in the second experiment this compartment was filled with an ^{123}I solution of approximately 20 MBq. In both experiments, the skull region was filled with the K_2HPO_4 solution at the concentration suggested by de Dreuille et al. [14] (100 g of K_2HPO_4 diluted to 67 g of distilled water). The SPECT acquisition followed a standardized protocol for clinical CBF quantitation using ^{123}I-iodoamphetamine, as recently described [17]. Seven frames of a dynamic SPECT scan were acquired over a 28-min period at 4 min per frame. The matrix size was 64 × 64, and the number of projection data was 90. Before the reconstruction, all projection data were summed over the whole period, normalized for detector non-uniformity, and calibrated for the centre-of-rotation using the standard vendor software. Then, these data were reconstructed using the QSPECT reconstruction program, including the attenuation correction and scatter correction procedures, as recently described by Iida et al. [17]. A single threshold level (% of the peak of projection data), which was consistent with that in a clinical study, was assigned to define the head contour and generate a uniform attenuation coefficient map. Reconstructed SPECT images were calibrated in Bq/mL, which provides independence from the scanning parameters such as the acquisition time, number of views, matrix size, zoom factor, etc. [17].

Scans were also performed on a phantom using a ECAT ACCEL PET scanner (Siemens-CTI, Knoxville, TN, USA), which provides an intrinsic spatial resolution of 4.5 mm full-width at half-maximum (FWHM) at the centre